

# Synthesis, Electrochemistry, and Optical Properties of Highly Conjugated Alkynyl-Ferrocenes and -Biferrocenes

Troy L. R. Bennett, Luke A. Wilkinson,\* Jasmine M. A. Lok, Robert C. P. O'Toole, and Nicholas J. Long\*



Cite This: *Organometallics* 2021, 40, 1156–1162



Read Online

ACCESS |



Metrics & More

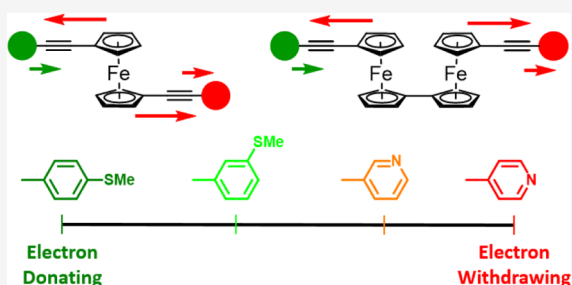


Article Recommendations



Supporting Information

**ABSTRACT:** Sonogashira reactions are utilized herein to react iodoferrocenes and -biferrocenes with terminal alkyne ligands, functionalized with both pyridine and thioanisole groups. High-yielding reactions generate both monoalkynyl and dialkynyl derivatives, the ratio of which can be altered through changes in the reaction stoichiometry. This methodology allowed us to synthesize a large family of derivatives, comprising four symmetrical derivatives (3xx, where x represents a phenyl-substituted terminal alkyne) and six less-studied asymmetrical derivatives (3xy, where x and y represent two different phenyl-substituted terminal alkynes), as well as a number of their biferrocenyl analogues (6x, 7xx, and 7xy), including the first known examples of asymmetrically disubstituted biferrocenes. We examined the electrochemical behavior of all the systems in solution through the use of cyclic voltammetry and demonstrate that these highly conjugated alkynyl ligands exert delicate redox control over the central ferrocene motif. We also note that these substituents display some control over the mixed-valence character present in biferrocene monocations, with thioanisole substituents imparting almost an order of magnitude higher  $K_c$  than their pyridyl analogues, and asymmetric systems displaying rare characteristic properties of mixed-valence isomers. The electronic structure of these systems was further elucidated through a combination of UV/vis spectroscopy and density functional theory calculations. Our methodology provides a facile and adaptable route toward the isolation of a number of novel ferrocene and biferrocene derivatives. From our perspective, the asymmetric nature of these systems, along with the delicate and predictable redox control that these ligands exert on the central ferrocene unit(s), could lead to applications in molecular electronics, where these properties have previously shown promise in the fabrication of diodes and rectifiers, as well as in the synthesis of donor- $\pi$ -acceptor systems.



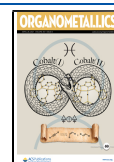
## INTRODUCTION

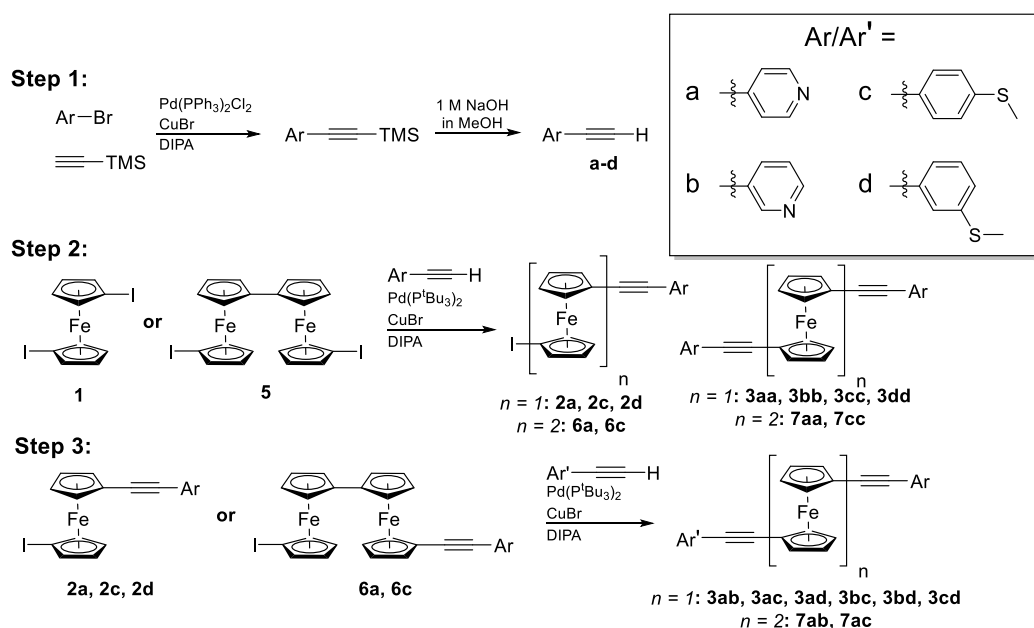
The desire to introduce a well-defined redox center, such as ferrocene, into a wide-ranging array of molecules, has led to the development of a rich library of new synthetic methods.<sup>1,2</sup> This abundance of techniques has resulted in ferrocene derivatives being incorporated into a wide variety of fields including catalysis, materials science, medicine, and a large number of different electrochemical applications.<sup>3–9</sup> One relatively recent addition to this synthetic tool kit was the synthesis and isolation of 1,1'-diiodoferrocene in high yields, which has been demonstrated within our group, through the use of an “oxidative purification” methodology, as well as by Nijhuis *et al.* who utilized a sublimation-focused route.<sup>10,11</sup> Both of these methods generate the highly versatile synthon and its biferrocene equivalent (1,1''-diiodobiferrocene) in high yields and with a high degree of purity. The realization of these synthons has opened up the use of classical cross-coupling methodologies. In particular, Sonogashira cross-couplings of iodoferrocenes present a valuable opportunity for the synthesis of highly conjugated redox-active molecules through reactions with terminal alkynes. Through substitution of alkynyl moieties

onto a ferrocene center, we can create a robust, highly conductive structure with the ability to rotate around a central node. These attractive properties have led to the application of these systems in the fabrication of highly ordered macromolecular assemblies and more prominently in the design and fabrication of electronic materials and single-molecule wires.<sup>12–20</sup> However, to date, most studies of ferrocene in these contexts have focused on the synthesis and study of small families of monosubstituted and symmetrically disubstituted systems, potentially owing to the relative ease of their synthesis and purification.<sup>21–28</sup> Although impressive, these studies have often been limited in scope and ignore the potential that asymmetry could impart on the electronic and structural properties of these species. For instance, research in the field of

Received: February 18, 2021

Published: April 12, 2021



Scheme 1. Synthetic Pathway Used in the Assembly of Ferrocene and Biferrocene Compounds Disubstituted in Each Case with Two Ethynyl-Arene Substituents<sup>a</sup>

<sup>a</sup>“Step 1” denotes the formation of the ethynyl-arene ligands, “step 2” denotes the initial reactions with 1,1'-diiodoferrocene and 1,1''-diiodobiferrocene to form a statistical mixture of mono- and disubstituted ferrocenes, and “step 3” shows subsequent reactions that were utilized to introduce asymmetry across the central ferrocenyl units.

molecular electronics has provided a number of examples where the asymmetric design has been applied in the fabrication of systems for molecular rectification and has also been demonstrated as an effective tool for tailoring different ends of a molecule to different electrode materials.<sup>29–33</sup> In an effort to bridge this gap between synthesis and design, we constructed an adaptable synthetic route that could be applied in the isolation of a large number of new asymmetric ferrocenyl derivatives. For this, we selected four different “ligands” with subtly different chemical, and by extension, electronic structures, these being 4-ethynylpyridine (a), 3-ethynylpyridine (b); 4-ethynylthioanisole (c), and 3-ethynylthioanisole (d). Herein, we demonstrate a facile and scalable synthesis of a series of novel symmetric and asymmetric alkynyl-ferrocenes and -biferrocenes. We examined the properties of these systems through a combination of electrochemistry, UV/vis, and computational methods, demonstrating a predictable redox tunability within the family, as well as uncovering rare examples of mixed-valence isomers.

## ■ SYNTHESIS

Synthesis of each compound was achieved via an iterative Sonogashira coupling process, using a methodology that has previously found success in our group.<sup>34</sup> The arylbromide [ArBr, where Ar = 4-pyridyl (a), 3-pyridyl (b), 4-thioanisole (c), or 3-thioanisole (d)] was coupled to trimethylsilylacetylene and subsequently deprotected to yield the terminal alkynes in high yields. From here, it was possible to couple the functionalized alkynes to 1,1'-diiodoferrocene (1). In this step (Scheme 1, step 2), access to both the monosubstituted products (2x) and the symmetrically disubstituted products (3xx) can be achieved through careful control of reaction stoichiometry. To preferentially obtain the monosubstituted products (2x), an excess of diiodoferrocenes must be employed (this is easily recovered after the reaction through

column chromatography) and the converse is true when aiming for the symmetrical doubly substituted products (3xx). Compounds 2x can then be taken forward in an additional coupling step to obtain the asymmetric disubstituted products (e.g., 3xy). Conveniently, multiple derivatives can be obtained in a one-pot reaction of a monosubstituted ferrocene (2x) with two different alkynes, although this leads to a statistical mixture of products, as is seen in the synthesis of 3bc and 3cd (see Supporting Information). Purification is largely facile; however, the pyridyl-based analogues require separation on a short alumina(V) column due to their propensity to streak on silica. For this reason, it was beneficial to prepare the asymmetric variants in a stepwise manner, starting from the thioanisole precursors (2c or 2d) in order to maximize yield and ease of purification. For comparative purposes, the ferrocenyl derivatives containing only one arm [i.e., CpFe(C<sub>5</sub>H<sub>4</sub>CCAr) (4) where Ar = 4-pyridyl or 4-thioanisole] were synthesized from ethynyl-ferrocene according to Scheme 1, step 2 to generate 4a and 4c, respectively. This methodology was extended to the synthesis of a select number of biferrocenyl derivatives through reaction of 1,1''-diiodobiferrocene (5) with both (a) and (c). This, once again, produced a mixture of monosubstituted (6x) and disubstituted (7xx) products, which could be isolated through the use of column chromatography. The yields of the biferrocene reactions were somewhat reduced in comparison to their monoferrocene counterparts, which we attribute to decreased reactivity of the biferrocenyl centers. Molecules (6x) were then substituted with different alkynes to produce asymmetric biferrocene derivatives (7xy), which would have been difficult to isolate through currently available biferrocene functionalization methods.<sup>34</sup> All compounds have been characterized by mass spectrometry and their bulk purity was determined through elemental analysis where possible. This synthesis was aided throughout by excellent resolution within the <sup>1</sup>H NMR spectra, whereby all compounds show the

expected number of pseudo-triplet signals associated with the ferrocene Cp protons at 4.0–4.8 ppm. For the symmetrical monoferrocene species (3aa–dd), these present as two pseudo-triplets, whereas four distinct pseudo-triplets are observed for the asymmetric variants (e.g., 3ac). When extending this analysis to the biferrrocene family, once again, very distinct profiles can be observed in the  $^1\text{H}$  NMR spectra with the symmetrical biferrrocenes producing four pseudo-triplets and the asymmetric systems producing eight (Figure 1).

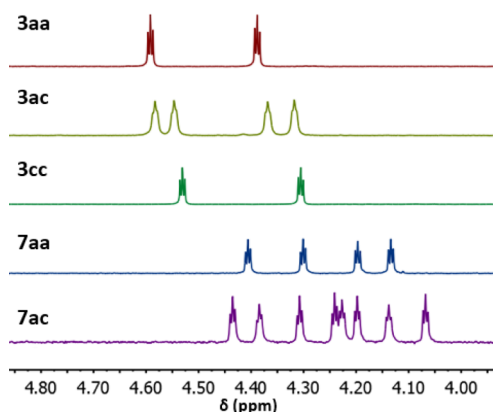


**Figure 1.** Comparative  $^1\text{H}$  NMR spectra of different compounds, illustrating various Cp-H environments that arise from both asymmetry and the inclusion of multiple ferrocene units.

## ELECTROCHEMISTRY

Cyclic voltammetry (CV) experiments were performed on all molecules in dichloromethane solutions with 0.1 M  $\text{N}^n\text{Bu}_4\text{PF}_6$  as the supporting electrolyte, and the relevant data are reported in Table 1 (monoferrocenes) and Table 2 (biferrrocenes). Looking first at the monoferrocene compounds, these all displayed a characteristic one-electron redox process, associated with the ferrocene motif, at potentials, which are more positive than that of standard ferrocene.<sup>35,36</sup> This is a consequence of the ethynylarene substituents, which withdraw electron density from the redox-center by extending the  $\pi$ -

**Table 1.** CV Data Obtained for Complexes 3xx and 4x in Solution<sup>a</sup>

[Fc]	$E_p$	$E_c$	$E_{1/2}$	$\Delta E$	$i_{pa}/i_{pc}$
3aa	336	264	300	72	1.23
3ab	319	249	284	70	1.06
3ac	247	182	215	65	1.08
3ad	284	213	249	71	1.11
3bb	296	209	253	87	1.05
3bc	246	172	209	74	1.02
3bd	268	188	228	80	0.89
3cc	196	130	163	66	0.93
3cd	196	130	163	66	0.86
3dd	237	173	205	64	1.00
4a	195	127	161	68	0.98
4c	135	69	102	66	0.94

<sup>a</sup>0.1 M  $\text{N}^n\text{Bu}_4\text{PF}_6$  in  $\text{CH}_2\text{Cl}_2$  taken at  $100\text{ mV s}^{-1}$  with a glassy carbon working electrode and a Pt wire as reference and counter electrodes. All potentials (mV) are reported vs  $\text{Fc}/\text{Fc}^+$  and have been corrected for  $iR_s$  with values obtained from AC impedance measurements.

**Table 2.** CV Data Obtained for Complexes 6x and 7xx in Solution<sup>a</sup>

[Fc <sub>2</sub> ]	$E_p$	$E_c$	$E_{1/2}$	$\Delta E$	$i_{pa}/i_{pc}$	$\Delta E_{1E_2}$	$K_c$
6a	64	-23	44	87	1.15	303	$10^{5.12}$
	415	279	347	136			
6c	13	-71	-29	84	0.95	366	$10^{6.19}$
	378	295	337	83			
7aa*	3	-57	-27	60	0.51	303	$10^{5.12}$
	322	230	276	92			
7ab*	4	-66	-31	70	0.62	325	$10^{5.50}$
	347	241	294	106			
7ac	49	-56	-34	105	1.04	370	$10^{6.26}$
	391	287	336	109			
7cc	-21	-103	-62	82	0.95	353	$10^{5.97}$
	330	253	291	78			

<sup>a</sup>0.1 M  $\text{N}^n\text{Bu}_4\text{PF}_6$  in  $\text{CH}_2\text{Cl}_2$  taken at  $100\text{ mV s}^{-1}$  with a glassy carbon working electrode and a Pt wire as reference and counter electrodes. All potentials (mV) are reported vs  $\text{Fc}/\text{Fc}^+$  and have been corrected for  $iR_s$  with values obtained from AC impedance measurements.

system; a fact that is nicely evidenced by comparing the potentials of, for example, 3cc and 4c. Additionally, the substituents on the arene were found to exert a significant influence on the overall potential and reversibility of the redox process. The molecules that incorporate only thioanisole groups (Xc/d) undergo redox chemistry that is both chemically ( $i_{pa}/i_{pc} \approx 1$ ) and electrochemically reversible ( $\Delta E \approx 65\text{ mV}$  over multiple scan rates), with diffusion-controlled electron transfer rates ( $i_p \propto \nu^{1/2}$ ).<sup>37</sup> Changes in redox potential can be observed between the 3-(3dd) and 4-substituted (3cc) thioanisole compounds, with 3-thioanisoles occurring at a higher potential than their 4-substituted analogues. A rationale for this stems from the ability of the thiomethyl moiety to donate electrons into the  $\pi$ -system and stabilize a positive charge. A qualitative analysis of the relevant resonance forms indicates that the positive charge is delocalized more effectively in the presence of the 4-thioanisole than the 3-thioanisole, thus reflecting the trend observed in the data. A similar, yet opposite trend is observed for the series containing only pyridyl groups (3a/b). The 3-pyridyl moiety is able to stabilize the positive charge to a greater degree than the corresponding 4-pyridyls, with the analogue containing both groups (3ab) displaying an intermediate potential. The trend in the redox potentials of this series reflects those in both the pyridyl- and thioanisole-based analogues, such that a continuum of potentials can be observed across the whole series of molecules (Figure 2). Thus, while the net effect of the arylalkynes is

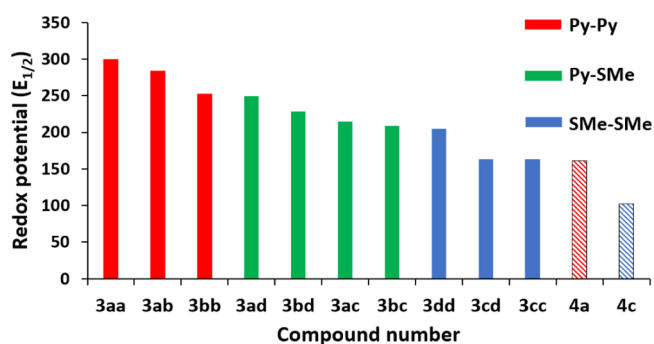


**Figure 2.** Redox potentials (mV) of compounds 3xx (solid bar) and 4x (striped bar).

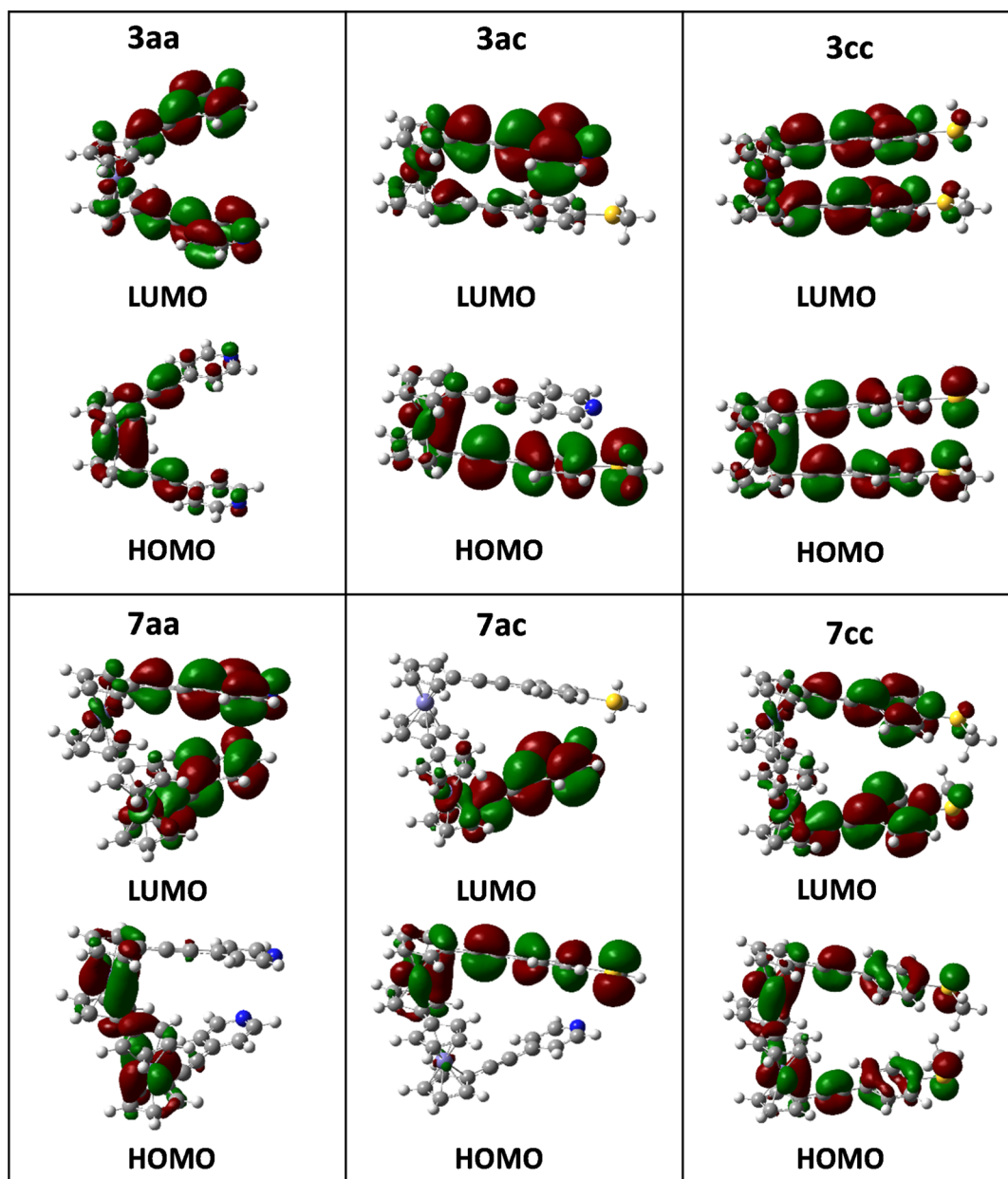


**Figure 3.** FMOs for a number of compounds that illustrate the differences in the formation of the HOMOs and LUMOs that result from the addition of an additional ferrocene motif and also from introducing asymmetry across the ferrocene unit.

electron-withdrawing, the redox properties of the ferrocene can be tuned further by varying the electron-donating/-withdrawing properties of the arene. Turning now to examine the biferrrocene systems **6x** and **7xx/xy**. All show two distinct redox processes and we attribute these redox features to the sequential oxidation of the two  $\text{Fe}^{2+}/\text{Fe}^{3+}$  couples present in each system.<sup>21</sup> Compounds **7aa** and **7cc** are fully symmetrical systems so the separation between the two redox processes ( $\Delta E_{1/2}$ ) can be attributed to charge stabilization via electronic coupling between the two ferrocene centers in the mixed-valence ion (e.g.,  $[\text{Fe}^{\text{II}}-\text{Fe}^{\text{III}}]^+$ ). The stability of this mixed-valence ion can be inferred from the comproportionation constant ( $K_c$ ) for the equilibrium between the mixed-valence ion, and its neutral and doubly oxidized forms, and can be derived from the Nernst equation, according to eq 1.

$$K_c = 10^{(F \cdot \Delta E_{1/2} / 2.303 \cdot RT)} \quad (1)$$

Using the potentials obtained from the CV of **7aa** and **7cc**, we can determine  $K_c$  as  $1.3 \times 10^5$  and  $9.3 \times 10^5$ , respectively, suggesting that they belong to class III of the Robin and Day series. For compounds **6x**, **7ab**, and **7ac**, these calculations become more complicated due to the asymmetric structure of the molecules. The monoferrrocenes described previously (**3xx/xy** and **4x**) clearly show that the redox properties of an individual ferrocene center can be influenced by substituents on the Cp ring. Therefore, it is incorrect to consider these biferrrocene units as simple mixed-valence systems, rather they are rare examples of mixed-valence isomers.<sup>38</sup> In such systems,  $\Delta E_{1/2}$  is no longer purely a consequence of coupling between redox centers, but is also affected by the intrinsic potential difference between the two independent redox sites.<sup>39</sup> A consequence of this is that  $\Delta E_{1/2}$  values obtained from the CV of mixed-valence isomers can provide an overestimation of the electronic coupling present within the system. To illustrate

this, the redox profile of biferrocene **7ac** can be compared to those of monoferrocenes **4a** and **4c**. **4a** is oxidized at 161 mV, while **4c** is oxidized at 102 mV, which gives  $\Delta E_{4a/4c} = 59$  mV.  $\Delta E_{1/2}$  of **7ac** is 370 mV and approximately 59 mV of that must come from the intrinsic potential difference between the two independent ferrocene centers. This means that only around 311 mV ( $=370-59$ ) can be attributed to stabilization via electronic coupling. Gratifyingly, this value of 311 mV is intermediate between those of the analogous symmetrical biferrocenes **7aa** (303 mV) and **7cc** (353 mV). While care must be taken to compare “like-for-like” systems,<sup>34</sup>  $K_c$  is often used as an indicator of coupling strength in mixed-valence systems. However, due to the redox asymmetry present in **6x**, **7ab**, and **7ac**,  $K_c$  cannot be employed in this way. A more in-depth investigation into the electronics of these mixed-valence isomers is currently underway in our laboratory.

## ■ INVESTIGATING THE ELECTRONIC STRUCTURE

To investigate the electronic structure of this series, a combination of theoretical calculations and UV/vis spectroscopy was employed. For this, the most stable ground-state geometry of each compound was determined by density functional theory (DFT) calculations in the gas phase, using the B3LYP functional and the 6-311+G(d,p) basis set. In addition, time-dependent DFT (TD-DFT) calculations, used to model the UV/vis spectra, employed the aforementioned optimized geometries and were performed using a dichloromethane conductor-like solvent polarization continuum model (CPCM) with the PBE1 functional and the 6-31+G(d,p) basis set to generate results that could be compared to the experimental spectra obtained in the same solvent (see [Supporting Information](#)). A few initial conclusions could be drawn from the experimental UV/vis spectra. For instance, it has previously been reported that unsubstituted ferrocene displays a transition at approximately 442 nm, which relates to two overlapping spin-allowed, Laporte forbidden transitions.<sup>40</sup> We see that, in all cases, our introduction of alkynyl ligands causes a bathochromic shift of this peak to higher wavelengths (between 445 and 460 nm), coinciding with previous work in the literature, which suggests that inclusion of an alkyne substituent acts to decrease the highest occupied molecular orbital (HOMO)–lowest unoccupied molecular orbital (LUMO) gap.<sup>41–43</sup> This is clearly demonstrated when comparing molecules **4a** and **4c**, where the more electron-withdrawing pyridyl causes a larger shift, though the trend becomes far less distinct upon introduction of a second alkynyl substituent. Trends relating to other ferrocene-associated transitions are harder to quantify as these are often obscured by large intense absorptions that occur between 250 and 325 nm. Analysis of the frontier molecular orbital (FMO) energies and their iso-surfaces as determined by DFT calculations, alongside the predicted absorption spectra (as modeled by TD-DFT calculations) provided further useful insights into the nature of these optical transitions. Our calculations suggest that the lower energy signals that appear around 450 nm are primarily metal-to-ligand charge transfer (MLCT) in character, while those around 350 nm result from transitions between orbitals that are more delocalized across the whole molecule and are essentially  $\pi \rightarrow \pi^*$  in character. The absorption bands observed at lower wavelengths can be assigned to higher-energy  $\pi \rightarrow \pi^*$  transitions, though it should be noted that those molecules containing two different arylalkyne substituents display a significant degree of interligand charge transfer

that also contributes to the overall signals below 350 nm. In most cases, the HOMO and LUMO are somewhat delocalized across the whole molecule, although in pyridyl-based analogues there is a clear bias toward a ferrocene-based HOMO and a LUMO situated on the ethynylpyridine. In addition to this, the FMOs of those systems containing both a pyridine and a thioanisole substituent seem to show particular favorability for the HOMO to be localized on the thioanisole fragment and the LUMO to be localized on the pyridyl fragment as is particularly evident in the FMOs of **3ac** and **7ac** ([Figure 3](#)). When considering the biferrocene systems, the UV/vis analysis demonstrates that these show similar transitions to their monoferrocene analogues, with the primary difference being a general increase in their intensity. The TD-DFT data suggests that the majority of these transitions are dominated by complex MLCT processes (see e.g., [Table S14](#)). Finally, it is also worth noting that an analysis of the FMO energies of these systems generated a trend in the energy of the HOMOs, which mirrored that which was observed in the redox potentials of our systems as reported above ([Figure S83](#)), suggesting that a predictable redox tunability exists within this family. Energy level diagrams, iso-surface depictions of the FMOs, and a list of predicted transitions, with their full assignments, for each compound, are provided in the [Supporting Information](#).

## ■ CONCLUSIONS

Herein, we have shown a facile synthesis of a large library of novel, highly conjugated, alkynyl-substituted ferrocene and biferrocene derivatives that have been fully characterized. Cyclic voltammetry was used to examine the electronic structure of these systems and it was shown that the differing substitution patterns impart fine redox control over the central ferrocene unit(s). The biferrocene molecules display subtly different mixed-valence character, with **7ac**, and likely **7ab**, displaying the characteristics of rare mixed-valence isomers. A combination of UV/vis spectroscopy and theoretical calculations, derived from DFT, was used to further elucidate the electronic structure of these compounds, providing clear justification for the redox tuning as a function of HOMO energy, occurring in a highly predictable manner. This analysis also allowed us to analyze the optical transitions observed for these compounds, noting a variety of complex MLCT processes, with those asymmetric systems containing both pyridyl and thioanisole fragments displaying more interligand charge transfer characteristics than their symmetrically substituted counterparts. Broadly speaking, this work demonstrates the ease and practicality of introducing asymmetry across a redox-center and how this can be used to subtly alter said center's electronic structure. Asymmetric molecules have previously shown promise in the field of molecular electronics in devising new systems for diodes, rectifiers, and in the tuning of optical band gaps.<sup>44–51</sup> The stepwise nature of our synthesis provides a routine method of incorporating an organometallic redox-active fragment into these designs and also provides an opportunity to study how their properties can be changed by externally controlling the ferrocene redox processes through the use of electrochemical gating.<sup>52–55</sup> In addition, this fine control of electronic structure provides a further parameter for the predictable tuning of FMO energies, which has large implications in both electronic and thermal conductivity as both are highly dependent on the alignment of the energy levels of electrodes and analytes.<sup>56–61</sup> We are currently undertaking further work to examine how these molecules

can be assembled onto a surface and how they differ in terms of their conductivity when studied as either single molecules or as parallel arrays of molecules, such as those seen in a self-assembled monolayer.

## ■ ASSOCIATED CONTENT

### Supporting Information

The Supporting Information is available free of charge at <https://pubs.acs.org/doi/10.1021/acs.organomet.1c00098>.

Experimental details including full synthetic procedures, spectroscopic data, cyclic voltammetry data, and ultraviolet–visible spectroscopy data as well as full molecular orbital depictions and energy levels for all molecules (PDF)

Calculated molecular coordinates of ferrocenes (XYZ)

## ■ AUTHOR INFORMATION

### Corresponding Authors

Luke A. Wilkinson – Department of Chemistry, University of York, York YO10 5DD, U.K.; [orcid.org/0000-0002-8550-3226](https://orcid.org/0000-0002-8550-3226); Email: [luke.a.wilkinson@york.ac.uk](mailto:luke.a.wilkinson@york.ac.uk)

Nicholas J. Long – Department of Chemistry, Imperial College London, London W12 0BZ, U.K.; [orcid.org/0000-0002-8298-938X](https://orcid.org/0000-0002-8298-938X); Email: [n.long@imperial.ac.uk](mailto:n.long@imperial.ac.uk)

### Authors

Troy L. R. Bennett – Department of Chemistry, Imperial College London, London W12 0BZ, U.K.

Jasmine M. A. Lok – Department of Chemistry, University of York, York YO10 5DD, U.K.

Robert C. P. O'Toole – Department of Chemistry, University of York, York YO10 5DD, U.K.

Complete contact information is available at:

<https://pubs.acs.org/doi/10.1021/acs.organomet.1c00098>

### Notes

The authors declare no competing financial interest.

## ■ ACKNOWLEDGMENTS

The authors acknowledge funding from the EPSRC (L.A.W. for EP/N032977/2 and TLRB for studentship 2033057), and N.J.L. is grateful for a Royal Society Wolfson Research Merit Award. L.A.W. is also grateful to the Leverhulme Trust for an Early Career Fellowship ECF-2019-134. This article is dedicated to Professor Wolfgang Kaim on the occasion of his 70th birthday, and to acknowledge his outstanding contributions to inorganic coordination chemistry and the understanding of mixed-valency and electron transfer.

## ■ REFERENCES

- (1) Astruc, D. Why Is Ferrocene so Exceptional? *Eur. J. Inorg. Chem.* **2017**, 6–29.
- (2) Heinze, K.; Lang, H. Ferrocene - Beauty and Function. *Organometallics* **2013**, *32*, 5623–5625.
- (3) Atkinson, R. C. J.; Gibson, V. C.; Long, N. J. The Syntheses and Catalytic Applications of Unsymmetrical Ferrocene Ligands. *Chem. Soc. Rev.* **2004**, *33*, 313–328.
- (4) Maheshwari, H.; Vilà, N.; Herzog, G.; Walcarius, A. Selective Detection of Cysteine at a Mesoporous Silica Film Electrode Functionalized with Ferrocene in the Presence of Glutathione. *ChemElectroChem* **2020**, *7*, 2095–2101.
- (5) Patra, M.; Gasser, G. The Medicinal Chemistry of Ferrocene and Its Derivatives. *Nat. Rev. Chem.* **2017**, *1*, 0066.

- (6) Nijhuis, C. A.; Reus, W. F.; Whitesides, G. M. Mechanism of Rectification in Tunneling Junctions Based on Molecules with Asymmetric Potential Drops. *J. Am. Chem. Soc.* **2010**, *132*, 18386–18401.

- (7) Saleem, M.; Yu, H.; Wang, L.; Zain-ul-Abdin; Khalid, H.; Akram, M.; Abbasi, N. M.; Huang, J. Review on Synthesis of Ferrocene-Based Redox Polymers and Derivatives and Their Application in Glucose Sensing. *Anal. Chim. Acta* **2015**, *876*, 9–25.

- (8) Makhoul, R.; Gluyas, J. B. G.; Vincent, K. B.; Sahnoune, H.; Halet, J.-F.; Low, P. J.; Hamon, J.-R.; Lapinte, C. Redox Properties of Ferrocenyl Ene-Diynyl-Bridged Cp\*(Dppe)M-C≡C-1,4-(C6H4) Complexes. *Organometallics* **2018**, *37*, 4156–4171.

- (9) Gagne, R. R.; Koval, C. A.; Lisensky, G. C. Ferrocene as an Internal Standard for Electrochemical Measurements. *Inorg. Chem.* **1980**, *19*, 2854–2855.

- (10) Inkpen, M. S.; Du, S.; Driver, M.; Albrecht, T.; Long, N. J. Oxidative Purification of Halogenated Ferrocenes. *Dalton Trans.* **2013**, *42*, 2813–2816.

- (11) Roemer, M.; Nijhuis, C. A. Syntheses and Purification of the Versatile Synthons Iodoferrocene and 1,1'-Diiodoferrocene. *Dalton Trans.* **2014**, *43*, 11815–11818.

- (12) Vasdev, R. A. S.; Findlay, J. A.; Garden, A. L.; Crowley, J. D. Redox Active [Pd2L4]4+cages Constructed from Rotationally Flexible 1,1'-Disubstituted Ferrocene Ligands. *Chem. Commun.* **2019**, *55*, 7506–7509.

- (13) Hoffmann, V.; le Pleux, L.; Häussinger, D.; Unke, O. T.; Prescimone, A.; Mayor, M. Deltoid versus Rhomboid: Controlling the Shape of Bis-Ferrocene Macrocycles by the Bulkiness of the Substituents. *Organometallics* **2017**, *36*, 858–866.

- (14) Hoffmann, V.; Jenny, N.; Häussinger, D.; Neuburger, M.; Mayor, M. Rotationally Restricted 1,1'-Bis(Phenylethynyl)Ferrocene Subunits in Macrocycles. *Eur. J. Org. Chem.* **2016**, 2187–2199.

- (15) Yuan, Y.; Yan, J.-F.; Lin, D.-Q.; Mao, B.-W.; Yuan, Y.-F. Ferrocene-Alkynyl Conjugated Molecular Wires: Synthesis, Characterization, and Conductance Properties. *Chem. Eur. J.* **2018**, *24*, 3545–3555.

- (16) Dong, T.-Y.; Chen, K.; Lin, M.-C.; Lee, L. Toward the Development of Molecular Wires: Ruthenium(II) Terpyridine Complexes Containing Polyferrocenyl as a Spacer. *Organometallics* **2005**, *24*, 4198–4206.

- (17) Vincent, K. B.; Gluyas, J. B. G.; Zeng, Q.; Yufit, D. S.; Howard, J. A. K.; Hartl, F.; Low, P. J. Sandwich and Half-Sandwich Metal Complexes Derived from Cross-Conjugated 3-Methylene-Penta-1,4-Diynes. *Dalton Trans.* **2017**, *46*, 5522–5531.

- (18) Haque, A.; Al-Balushi, R. A.; Al-Busaidi, I. J.; Khan, M. S.; Raithby, P. R. Rise of Conjugated Poly-Ynes and Poly(Metalla-Ynes): From Design through Synthesis to Structure-Property Relationships and Applications. *Chem. Rev.* **2018**, *118*, 8474–8597.

- (19) Dong, Q.; Meng, Z.; Ho, C.-L.; Guo, H.; Yang, W.; Manners, I.; Xu, L.; Wong, W.-Y. A Molecular Approach to Magnetic Metallic Nanostructures from Metallopolymer Precursors. *Chem. Soc. Rev.* **2018**, *47*, 4934–4953.

- (20) Ho, C.-L.; Yu, Z.-Q.; Wong, W.-Y. Multifunctional Poly-metalallaynes: Properties, Functions and Applications. *Chem. Soc. Rev.* **2016**, *45*, 5264–5295.

- (21) Gottwald, D.; Yuan, Q.; Speck, M.; Mahrholdt, J.; Korb, M.; Schreiter, K.; Spange, S.; Lang, H. Synthesis and (Spectro)-Electrochemistry of 1',1''-Disubstituted Biferrocenes. *J. Organomet. Chem.* **2020**, *923*, 121447.

- (22) Chen, C.-P.; Luo, W.-R.; Chen, C.-N.; Wu, S.-M.; Hsieh, S.; Chiang, C.-M.; Dong, T.-Y. Redox-Active  $\pi$ -Conjugated Organometallic Monolayers: Pronounced Coulomb Blockade Characteristic at Room Temperature. *Langmuir* **2013**, *29*, 3106–3115.

- (23) Han, L.-M.; Hu, Y.-Q.; Suo, Q.-L.; Luo, M.-H.; Weng, L.-H. Synthesis and Characterization of 1', 1''-Bis(Ethynyl)Biferrocenyl Derivatives. *J. Coord. Chem.* **2010**, *63*, 600–609.

- (24) Lohan, M.; Ecorchard, P.; Rüffer, T.; Justaud, F.; Lapinte, C.; Lang, H. 1,1'-Bis(Ethynyl)Biferrocene as a Linking Group for Gold, Ruthenium, and Osmium Fragments: Synthesis, Solid State

Structures, and Electrochemical, UV-Vis, and EPR Spectroscopic Studies. *Organometallics* **2009**, *28*, 1878–1890.

(25) Larik, F. A.; Saeed, A.; Fattah, T. A.; Muqadar, U.; Channar, P. A. Recent Advances in the Synthesis, Biological Activities and Various Applications of Ferrocene Derivatives. *Appl. Organomet. Chem.* **2017**, *31*, e3664.

(26) Lu, Q.; Yao, C.; Wang, X.; Wang, F. Enhancing Molecular Conductance of Oligo(p-Phenylene Ethynylene)s by Incorporating Ferrocene into Their Backbones. *J. Phys. Chem. C* **2012**, *116*, 17853–17861.

(27) Kanthasamy, K.; Ring, M.; Nettelroth, D.; Tegenkamp, C.; Butenschön, H.; Pauly, F.; Pfnür, H. Charge Transport through Ferrocene 1,1'-Diamine Single-Molecule Junctions. *Small* **2016**, *12*, 4849–4856.

(28) Fabre, B. Ferrocene-Terminated Monolayers Covalently Bound to Hydrogen-Terminated Silicon Surfaces. Toward the Development of Charge Storage and Communication Devices. *Acc. Chem. Res.* **2010**, *43*, 1509–1518.

(29) Galperin, M.; Nitzan, A.; Sek, S.; Majda, M. Asymmetric Electron Transmission across Asymmetric Alkanethiol Bilayer Junctions. *J. Electroanal. Chem.* **2003**, *550–551*, 337–350.

(30) He, C.; Zhang, Q.; Fan, Y.; Zhao, C.; Zhao, C.; Ye, J.; Dappe, Y. J.; Nichols, R. J.; Yang, L. Effect of Asymmetric Anchoring Groups on Electronic Transport in Hybrid Metal/Molecule/Graphene Single Molecule Junctions. *ChemPhysChem* **2019**, *20*, 1830–1836.

(31) Šebera, J.; Kolivoška, V.; Valášek, M.; Gasior, J.; Sokolová, R.; Mészáros, G.; Hong, W.; Mayor, M.; Hromádová, M. Tuning Charge Transport Properties of Asymmetric Molecular Junctions. *J. Phys. Chem. C* **2017**, *121*, 12885–12894.

(32) Ashwell, G. J.; Tyrrell, W. D.; Whittam, A. J. Molecular Rectification: Self-Assembled Monolayers in Which Donor-( $\pi$ -Bridge)-Acceptor Moieties Are Centrally Located and Symmetrically Coupled to Both Gold Electrodes. *J. Am. Chem. Soc.* **2004**, *126*, 7102–7110.

(33) Valdiviezo, J.; Palma, J. L. Molecular Rectification Enhancement Based on Conformational and Chemical Modifications. *J. Phys. Chem. C* **2018**, *122*, 2053–2063.

(34) Wilson, L. E.; Hassenrück, C.; Winter, R. F.; White, A. J. P.; Albrecht, T.; Long, N. J. Functionalised Biferrocene Systems towards Molecular Electronics. *Eur. J. Inorg. Chem.* **2017**, *2017*, 496–504.

(35) Paul, A.; Borrelli, R.; Bouyanif, H.; Gottis, S.; Sauvage, F. Tunable Redox Potential, Optical Properties, and Enhanced Stability of Modified Ferrocene-Based Complexes. *ACS Omega* **2019**, *4*, 14780–14789.

(36) Silva, M. E. N. P. R. A.; Pombeiro, A. J. L.; Fraústo da Silva, J. J. R.; Herrmann, R.; Deus, N.; Bozak, R. Redox Potential and Substituent Effects in Ferrocene Derivatives: II. *J. Organomet. Chem.* **1994**, *480*, 81–90.

(37) Elgrishi, N.; Rountree, K. J.; McCarthy, B. D.; Rountree, E. S.; Eisenhart, T. T.; Dempsey, J. L. A Practical Beginner's Guide to Cyclic Voltammetry. *J. Chem. Educ.* **2018**, *95*, 197–206.

(38) Salsman, J. C.; Kubiak, C. P.; Ito, T. Mixed Valence Isomers. *J. Am. Chem. Soc.* **2005**, *127*, 2382–2383.

(39) Xiao, X.; Liu, C. Y.; He, Q.; Han, M. J.; Meng, M.; Lei, H.; Lu, X. Control of the Charge Distribution and Modulation of the Class II-III Transition in Weakly Coupled Mo<sub>2</sub>-Mo<sub>2</sub> Systems. *Inorg. Chem.* **2013**, *52*, 12624–12633.

(40) Yamaguchi, Y.; Ding, W.; Sanderson, C. T.; Borden, M. L.; Morgan, M. J.; Kutal, C. Electronic Structure, Spectroscopy, and Photochemistry of Group 8 Metallocenes. *Coord. Chem. Rev.* **2007**, *251*, S15–S24.

(41) Long, N. J.; Martin, A. J.; Vilar, R.; White, A. J. P.; Williams, D. J.; Younus, M. Synthesis, Characterization, and Theoretical Studies of New Alkynylferrocene and -Biferrocene Ligands and Their Platinum-Containing Dimers and Oligomers. *Organometallics* **1999**, *18*, 4261–4269.

(42) Vacher, A.; Barrière, F.; Lorcy, D. Ferrocene and Tetrathiafulvalene Redox Interplay across a Bis-Acetylide-Ruthenium Bridge. *Organometallics* **2013**, *32*, 6130–6135.

(43) Bitter, S.; Kunkel, M.; Burkart, L.; Mang, A.; Winter, R. F.; Polarz, S. Organometallic, Nonclassical Surfactant with Gemini Design Comprising  $\pi$ -Conjugated Constituents Ready for Modification. *ACS Omega* **2018**, *3*, 8854–8864.

(44) Batra, A.; Darancet, P.; Chen, Q.; Meisner, J. S.; Widawsky, J. R.; Neaton, J. B.; Nuckolls, C.; Venkataraman, L. Tuning Rectification in Single-Molecular Diodes. *Nano Lett.* **2013**, *13*, 6233–6237.

(45) Lo, W.-Y.; Zhang, N.; Cai, Z.; Li, L.; Yu, L. Beyond Molecular Wires: Design Molecular Electronic Functions Based on Dipolar Effect. *Acc. Chem. Res.* **2016**, *49*, 1852–1863.

(46) Kumar, C.; Raheem, A. A.; Pandian, K.; Nandakumar, V.; Shanmugam, R.; Praveen, C. Fine-Tuning the Optoelectronic Channels of Fluoreno-Thiophene Centred Molecular Semiconductors through Symmetric and Asymmetric Push-Pull Switch. *New J. Chem.* **2019**, *43*, 7015–7027.

(47) Perrin, M. L.; Galán, E.; Eelkema, R.; Thijssen, J. M.; Grozema, F.; Van Der Zant, H. S. J. A Gate-Tunable Single-Molecule Diode. *Nanoscale* **2016**, *8*, 8919–8923.

(48) Zhang, G.; Ratner, M. A.; Reuter, M. G. Is Molecular Rectification Caused by Asymmetric Electrode Couplings or by a Molecular Bias Drop? *J. Phys. Chem. C* **2015**, *119*, 6254–6260.

(49) Liu, R.; Ke, S.-H.; Yang, W.; Baranger, H. U. Organometallic Molecular Rectification. *J. Chem. Phys.* **2006**, *124*, 024718.

(50) Chen, L.; Feng, A.; Wang, M.; Liu, J.; Hong, W.; Guo, X.; Xiang, D. Towards Single-Molecule Optoelectronic Devices. *Sci. China Chem.* **2018**, *61*, 1368–1384.

(51) Tsutsui, M.; Taniguchi, M. Single Molecule Electronics and Devices. *Sensors* **2012**, *12*, 7259–7298.

(52) Mishchenko, A.; Abdulla, M.; Rudnev, A.; Fu, Y.; Pike, A. R.; Wandlowski, T. Electrochemical Scanning Tunnelling Spectroscopy of a Ferrocene-Modified n-Si(111)-Surface: Electrolyte Gating and Ambipolar FET Behaviour. *Chem. Commun.* **2011**, *47*, 9807–9809.

(53) Xiao, X.; Brune, D.; He, J.; Lindsay, S.; Gorman, C. B.; Tao, N. Redox-Gated Electron Transport in Electrically Wired Ferrocene Molecules. *Chem. Phys.* **2006**, *326*, 138–143.

(54) Laucirica, G.; Marmisollé, W. A.; Toimil-Molares, M. E.; Trautmann, C.; Azzaroni, O. Redox-Driven Reversible Gating of Solid-State Nanochannels. *ACS Appl. Mater. Interfaces* **2019**, *11*, 30001–30009.

(55) Rudnev, A. V.; Zhumaev, U.; Utsunomiya, T.; Fan, C.; Yokota, Y.; Fukui, K.-i.; Wandlowski, T. Ferrocene-Terminated Alkanethiol Self-Assembled Monolayers: An Electrochemical and in Situ Surface-Enhanced Infra-Red Absorption Spectroscopy Study. *Electrochim. Acta* **2013**, *107*, 33–44.

(56) García-Suárez, V. M.; Lambert, C. J. Tailoring the Fermi Level of the Leads in Molecular-Electronic Devices. *Phys. Rev. B: Condens. Matter Mater. Phys.* **2008**, *78*, 235412.

(57) Xin, N.; Guan, J.; Zhou, C.; Chen, X.; Gu, C.; Li, Y.; Ratner, M. A.; Nitzan, A.; Stoddart, J. F.; Guo, X. Concepts in the Design and Engineering of Single-Molecule Electronic Devices. *Nat. Rev. Phys.* **2019**, *1*, 211–230.

(58) Stadler, R.; Jacobsen, K. W. Fermi Level Alignment in Molecular Nanojunctions and Its Relation to Charge Transfer. *Phys. Rev. B: Condens. Matter Mater. Phys.* **2006**, *74*, 164105.

(59) Zhao, X.; Stadler, R. DFT-Based Study of Electron Transport through Ferrocene Compounds with Different Anchor Groups in Different Adsorption Configurations of an STM Setup. *Phys. Rev. B* **2019**, *99*, 045431.

(60) Tanaka, Y.; Kato, Y.; Sugimoto, K.; Kawano, R.; Tada, T.; Fujii, S.; Kiguchi, M.; Akita, M. Single-Molecule Junction of Multinuclear Organometallic Wires: Long-Range Carrier Transport Brought About by Metal-Metal Interaction. *Chem. Sci.* **2021**, *12*, 4338.

(61) Frederiksen, T. Bimetallic Electrodes Boost Molecular Junctions. *Nat. Mater.* **2021**, DOI: 10.1038/s41563-021-00928-1.